End of the induction period in ordinary Portland cement as examined by high resolution scanning electron microscopy

Makar, J. M.; Chan, G. W.

Publisher's version / Version de l'éditeur:
https://doi.org/10.1111/j.1551-2916.2008.02304.x
Journal of the American Ceramic Society, 91, April 4, pp. 1292-1299, 2008-04-01

End of the induction period in ordinary Portland cement as examined by high-resolution scanning electron microscopy

NRCC-49236

Makar, J.M.; Chan, G.W.

A version of this document is published in / Une version de ce document se trouve dans: Journal of the American Ceramic Society, v. 91, no. 4, April 2008, pp. 1292-1299 doi: 10.1111/j.1551-2916.2008.02304.x

The end of the induction period in ordinary Portland cement as examined by high resolution scanning electron microscopy

Jon Makar[+] and G. Chan
Institute for Research in Construction,
National Research Council Canada
1200 Montreal Road, Ottawa, Ontario
K1A 0R6

[+]Corresponding author: jon.makar@nrc-cnrc.gc.ca

Abstract

The early stages of ordinary Portland cement (OPC) hydration were studied by cold field emission scanning electron microscopy and isothermal conduction calorimetry. Particular attention was paid to samples from the end of the induction period, where an additional peak in the tricalcium silicate hydration reaction has recently been discovered. Higher resolution images were obtained than is possible with current in-situ imaging techniques, allowing for the observation of features on the 5 nanometer scale. The peak in the hydration at the end of the induction period was associated with both the formation of pores in the surface of the cement grains and the formation of nanoscale C-S-H structures on those surfaces. The effects of grinding of OPC and additions of tricalcium aluminate and tetracalcium aluminoferrite on the peak at the end of the induction period were also examined. The results of the study were compared to the models in the literature used to describe the causes of the induction period and its end.

Introduction

Although the hydration of ordinary Portland cement (OPC) and its main constituent, $3CaO{\cdot}SiO_2$ (tricalcium silicate or C_3S in cement notation) have been studied extensively for many years[1], significant questions still remain about aspects of the hydration process. In particular, the nature of the induction period, a time of minimal chemical activity between initial reactions that occur upon wetting of the cement and the main C_3S hydration reaction remains unexplained. While there are a number of models in the literature for the events that take place during the dormancy period[2-12], there is no definitive consensus on the issue.

The models for the dormancy period and its end fall into two broad categories[13,14]. In the first group the dormancy period is believed to be caused by the formation of a protective shell on the surface of the OPC or C_3S grain at the time of wetting. The dormancy period ends when either the shell changes due to aging or phase transformation to allow water to access the grain or when internal osmotic pressure breaks down the shell. In the second group, no shell is formed. One model in this category has the dormancy period being caused by poisoning of the formation of calcium hydroxide (CH) by Si ions, with it ending when sufficient Ca ions become available to overcome the poisoning and allow the formation of CH. An alternative in this category assumes that C_3S does not truly exhibit a dormancy period as such and that instead there is a continuous, slow formation of calcium silicate hydrate (C-S-H) that gradually speeds up until a critical point is reached and reaction proceeds rapidly. Hybrid models have also been presented[14].

Recently, high resolution isothermal conduction calorimetry of C_3S hydration has shown that there is an additional reaction peak in the C_3S hydration process at the end of the induction period[15]. This "termination" peak had appeared occasionally in the literature[16], but had not previously been explained. Detection of the termination peak in isothermal conduction

calorimetry of standard cement samples requires very high resolution measurements both in terms of heat flow and measurement rate. As a result, repeatable measurements of the peak have only been possible with modern instrumentation. Differential scanning calorimetry measurements showed that the peak was associated with a change in rate of calcium hydroxide formation. High resolution cold field emission-scanning electron microscopy (CFE-SEM) examination of C_3S grains suggested that the termination hydration peak was produced due to the formation of pores in the surface of the C_3S grains and an associated rapid formation of calcium-silicate-hydrates (C-S-H). The association of the termination peak with surface behaviour was confirmed by additional conduction calorimetry tests that showed that the heat produced by the peak increased with increasing surface area of cement.

This paper presents the results of a complementary study of the early stages of the hydration of OPC and normal Portland cement (NPC) using isothermal conduction calorimetry and CFE-SEM, which demonstrates that the termination peak can also be observed during the hydration of these materials. The effects of grinding OPC and that of additions of tricalcium aluminate ($3CaO{\cdot}Al_2O_3$ or C_3A) and tetracalcium aluminoferrite ($4CaO{\cdot}Al_2O_3{\cdot}Fe_2O_3$ or C_4AF) on the termination peak are also examined. Although CFE-SEM does not allow for in-situ imaging, it does permit high resolution surface images to be obtained from the samples investigated without the need for surface coatings. The validity of the main classes of models for the induction period are then tested against the observed hydration behaviour.

Experimental Details

Two type 10 OPCs (manufactured by Lafarge in 2004 and St. Lawrence Cement in 2005) and one NPC (manufactured by Maritime in 1974) were examined. Rietveld analysis (Scintag XDS 2000) was used to determine the composition of each cement (Table 1). Five gram samples

of each cement were hydrated in polyethylene containers in a Thermometric Tam Air Isothermal Calorimeter (model 3114) using Accusolv (Anachemia, Inc.) water with a maximum impurity level of 1 ppm at a w/c ratio of 0.5 by mass at 23.0^{o} C. The results of the conduction calorimetry measurements were then plotted (Figure 1) and used to select specific times of hydration to be investigated by CFE-SEM. Additional conduction calorimetry measurements were obtained under the same conditions for samples of the Lafarge OPC ground to give a variety of surface areas and for both types of OPC mixed with increasing concentrations of analytical grade tricalcium aluminate (C_3A) and tetracalcium aluminoferrite (C_4AF). Surface areas of the ground material were measured using the BET method. Surface areas and percentages of C_3A and C_4AF are shown in the captions of the figures showing their effects on the hydration of OPC. The NPC was examined both because of its composition and because preliminary studies showed that it had been exposed to both carbon dioxide and water contamination during storage.

Additional one gram samples were then hydrated in the polyethylene containers at the same water to cement ratio using the same water supply and at the same temperature for each combination of cement and time to be investigated. Initial samples for imaging were prepared using an isopropanol based method of stopping hydration[17] and vacuum drying. Further samples were then prepared by freeze drying to produce the images shown here. Small amounts of cement removed from the center of the container at each time of interest. These small samples had their hydration stopped by placement in a vial in liquid nitrogen and were then kept under vacuum at liquid nitrogen temperatures until all of the water in the samples had sublimed. The latter samples were used for the images in this paper as freeze drying is believed to produce the best preservation of the original microstructure of cement samples[18,19].

Representative material from the center of each sample was extracted and distributed as individual grains across carbon tape attached to SEM aluminum stubs for imaging. A minimum of 16 grains from each sample were imaged in a Hitachi S-4800 cold field emission scanning electron microscope, with 32 grains being typical. Microscope parameters are shown in the figure captions. For the purposes of comparison to past SEM and environmental SEM studies, selected grains of OPC were imaged at both 2kV and 20kV, with a 4 μA current and a 4.9 mm working distance, the minimum possible to use in the instrument at the higher accelerating voltages. Where necessary, observed structures were also re-imaged at 20 kV and a 15 mm working distance in order to perform X-ray dispersive chemical analysis. No coatings were used in the imaging in order to avoid obscuring the details of the hydrating cement structures. Most images shown here were taken at 40,000x magnification, but samples were also imaged at a number of other magnifications and those images are used where appropriate.

Similar isothermal conduction calorimetry tests and CFE-SEM examinations were also performed on Type I/II, Type II and Type V OPC from a variety of suppliers in order to confirm the results described in this paper.

Results

Conduction Calorimetry

Figure 1 shows the conduction calorimetry hydration curves for the three cements that form the primary basis of the study, with Figure 1a showing the overall hydration behaviour and Figure 1b that within the first 300 minutes. Data were collected at 1 minute intervals, with the uncertainty being in the data being too small to show on the scale of the graph. The dots in Figure 1b represent the individual data points that were collected, while the larger symbols show the times where hydration was stopped to produce samples for imaging. Additional samples were

also prepared for imaging at 30, 240 and 360 minutes time. Only the final stages of the initial hydration reaction upon wetting are shown. All of the hydration curves show the effects of the surface reactions, identifiable by initial higher slopes of the main hydration peak in Figure 1b.

Figure 2a shows the effect of adding additional C_3A to the Lafarge 2004 OPC on its termination peak, while Figure 2b gives the equivalent data for additions of C_4AF. In Figure 2a increasing contents of C_3A increased the initial heat of hydration and gradually masked the heat flow produced by the termination peak, which appeared as a visible peak in the curve at 5% and 10% by weight added C_3A content, but as a flattening of the end of the C3A hydration peak for 15% and 20% by weight added C_3A content. The timing of the termination peak was not affected by the addition of the C_3A, having occurred between 90 and 140 minutes in all cases. However, increasing C_4AF content (Figure 2b) does affect the timing of the termination peak, with a 20% by weight addition of C_4AF delaying the onset of the peak by approximately 18 minutes. The size of the termination peak is reduced and the main hydration peak delayed, suggesting that the C_4AF addition acts as a weak retarder. Similar results were observed for the other OPC.

Figure 3 shows the effect of grinding the Lafarge 2004 OPC to produce higher surface areas, with the termination peak occurring earlier in time with higher fineness before becoming hidden by the increasing initial C_3A reaction. The termination peak was also observed for isothermal conduction calorimetry results from three type I/II OPCs, but was not visible in the results for a true Type II and Type V OPC.

Cold Field Emission Scanning Electron Microscopy

Most images presented in this section were obtained by examining the St. Lawrence 2005 ordinary Portland cement. These images are also representative of those obtained from the Lafarge 2004 OPC and the Maritime 1974 NPC. Minimal differences were observed between the

appearance of the two modern OPCs. Differences between OPC results and that of the NPC will be discussed below as appropriate. The same processes were also observed in the other OPCs examined in the study, including the Type II and Type V OPCs where the termination peak was not visible in the isothermal conduction calorimetry data. In those cases the timing of the physical events associated with the termination peak in the C_3S and Type I OPC samples occurred early enough in the hydration process that the corresponding isothermal conduction calorimetry event was masked by the heat of the C_3A hydration.

It should be noted that the description below is of typical cement grain behaviour. The hydration behaviour of individual Portland cement grains was clearly affected by local chemistry. Grains were observed in all cases that had hydrated more slowly or quickly than others in the same sample. While the CFE-SEM images show the general behaviour at any given time, the conduction calorimetry data in Figure 1 is a sum of the hydration behaviour around each of the grains, including those hydrating at substantially slower or faster rates.

a) Comparison between High and Low Voltage Results

Scanning electron microscopy images in the literature have typically been produced using at high accelerating voltages using either tungsten filament[20-24] or, more recently, environmental scanning electron microscopes[25-27]. The latter instruments have the advantage of being able to examine the cement samples without dehydration, allowing in-situ imaging. However, the 20-25 keV accelerating voltages that have typically been used may cause electrons to penetrate deeply into the surface of the cement sample, obscuring surface details. As an example, Figure 4a shows an image produced at 20 keV, while Figure 4b shows an image of the same structures taken at 2.0 keV. The level of detail obtained is much higher at the lower voltages and useful information can be obtained at higher magnifications than would otherwise be the case.

b) Structure of unhydrated cement

Figure 5 shows two examples of unhydrated OPC to illustrate the range of variation in observed surface morphologies. Most OPC grains had adhered smaller particles, as shown in both images. Many of these particles disappeared after the initial hydration, suggesting that they were composed of C_3A or one of the forms of calcium sulphate added to Portland cement in OPC to modify the C_3A reaction. Observed unhydrated OPC grains typically had smooth surfaces as shown at the top and bottom of Figure 5a, while the step-like structures in the center of the figure were not uncommon. These steps may have been produced by the effects of the grinding process on the monoclinic crystalline structure of C_3S. Other grains showed signs of substantial damage (Figure 5b). Examination of the "unhydrated" NPC showed that it had not been perfectly sealed during storage and had already experienced some degree of hydration, producing an appearance similar to that of Figure 6a described below.

c) Early age hydration sequence for Portland cement

After wetting, prismatic hydration products with an approximately hexagonal cross-section formed on the OPC and NPC grain surfaces (Figure 6a). While some of the same structures were already present on the surface of the NPC grains, additional hydration products were formed after that material was wetted. Their appearance immediately after wetting and their morphology, which has the appearance typical of ettringite[28,29], suggest that they were produced by the hydration of the calcium aluminate phase in the cement. X-ray diffraction measurements (not shown) confirmed the presence of ettringite in these samples. In some cases the prismatic structures covered most or all of the observed grain surface. Most observed samples resembled Figure 6a, with large surface areas that did not have visible hydration products. The prisms were observed in samples taken from each time of hydration.

Until the termination peak that marks the end of the induction period, most grains continued to show an appearance similar to that seen in Figures 6a. However, a few grains show some porosity and very small amounts of hydration products that appear to be C-S-H (Figure 6b). The latter, which appears in the figure as white rods (indicated by white arrows), is only identifiable at this stage by shape and degree of contrast with the other hydration products, being too small for elemental analysis. However, subsequent images show the transformation of this form of hydration product into structures that are recognizably C-S-H. The pores are typically 4-20 nm across in those areas where they appear at this stage of hydration.

Figures 6c and 6d show grain surfaces at 120 minutes of hydration, immediately after the termination peak. Pores were noticeably more common in the surfaces of the Portland cement grains (Figure 6c) and were sometimes much larger than those rare examples observed before the peak. The rod like hydration products are also more common and in some cases (Figure 6d) form in clusters on the surface of the grains.

By 180 minutes the sample was well past the termination peak and few if any of the grains retain the appearance seen in the Figures 6a. Some pores were much larger and deeper than those seen at 120 minutes (Figure 6e). Hydration products typically took the two forms at this point, either covering the surface of the cement grain with a criss-cross pattern of spikes (Figure 6f) or exhibiting clusters of spikes of increasing size (Figure 6g). By 240 minutes (Figure 6 h and i) all of the observed grains had had larger C-S-H clusters and pores present. Beyond this time, further growth of the C-S-H caused it to develop a morphology similar that reported previously as type I C-S-H[20].

d) Formation of Calcium Hydroxide

Occasional flat hexagonal crystals were seen on the surface of all the materials investigated both before and after the end of the induction period. Very small structures were seen before the end of the induction period (Figure 7, arrows), with much larger (5+ micrometers across) crystals identified after the end of the induction period. The larger crystals were confirmed as calcium hydroxide using energy dispersive analysis, but the structures in Figure 7 were too small for this technique to be applied. However, while the identified structures in Figure 7 could be composed of other hydration products, previous thermal analytical work[15] has confirmed that calcium hydroxide forms in hydrating cements well before the end of the induction period.

Discussion

The pore formation and C-S-H growth shown in Figure 6 was typical of all other investigated OPCs and was similar to that reported earlier for pure C_3S[15]. There were, however, significant differences between the isothermal calorimetry results for pure C_3S and those for OPC. In C_3S, the timing and the extent of the termination peak appears to be primarily controlled by the surface area of the cement particles. Higher surface areas produce an earlier and larger peak than smaller surface areas. In OPC, increasing surface area moves the termination peak forward in time (Figure 3) and may eventually move it under the peak from the initial C_3A hydration. There is little effect on the apparent size of the peak. Examining the results of adding C_3A (Figure 2a) to the OPC suggests that additional C_3A does not affect the timing of the peak, but may affect its extent. It is also possible that the heat generated by the additional C_3A is masking the termination peak. Additional C_4AF delays the onset of the peak and somewhat reduces its extent (Figure 2b).

Comparing the chemistry of the Portland cements examined here to the termination peaks shown in Figure 1b suggests that neither C_3A nor C_4AF has a direct effect on the termination peak. The two Portland cements with the highest C_4AF and C_3A contents (Lafarge 2004 and Maritime 1974 respectively) have more extensive termination peaks than the St. Lawrence 2005 OPC. Instead, the extent of the termination peak appears to be affected by the amount of surface area of the partially hydrated grains that were covered with hydration products after the initial C_3A reactions. Image analysis shows (Table 2) that the Lafarge 2004 OPC has the lowest covered surface area, followed by the Maritime 1974 NPC and then by the St. Lawrence OPC. Adding C_4AF or increasing the amount of C_3A available for reaction also increases the covered surface area. This analysis suggests the hydration products from the additional constituents in Portland cement act to reduce the surface area of the C_3S in the cement available for C-S-H nucleation reactions and thereby reduce the extent of the termination peak. Further work is needed to confirm this explanation.

While the C_3A and C_4AF affect the size of the termination peak, they do not appear to affect the hydration processes associated with it. The surface of the cement grains examined remained relatively intact throughout the induction period, with a few grains showing some porosity or minimal C-S-H formation. In all cases examined, the induction period ended with a process of rapid formation of pores in the grain surface, along with increasing levels of C-S-H formation, which created the "termination" peak in the hydration reactions shown in Figure 1b. Once the sites on the surface of the cement grains suitable for C-S-H nucleation or pore formation were consumed, the rate of hydration slowed somewhat due to a transition from surface behaviour to the volume based nucleation and growth of C-S-H. The process of pore formation and surface C-S-H growth was observed in all OPCs, although for the type II and V

OPCs, the initial C3A hydration period overlapped the time of the pore formation, apparently masking the presence of the termination peak.

The formation of C-S-H on the OPC grain surface was generally comparable to the observations of Henderson and Bailey[30], with the C-S-H structures visible in Figure 4g and the fine white spikes in the lower right corner of Figure 4e being of similar size and shape to their 3 and 7 hour observations. These structures may also correspond to the "sheaf of wheat structures reported in X-ray microscopy samples[31,32]. Similar structures were seen on other cement grains. Other structures reported by Henderson and Bailey may represent cross-sectional views of the C-S-H clusters seen here.

Previous workers have not reported the pores seen in Figures 6 and 8, although Ménétrier and co-workers[23] noted similar structures at a much larger scale. The pores initially had a diameter of 4 nm or less, at or below the resolution of the CFE-SEM on these materials. They quickly appeared on a few grains, but the vast majority of the pore formation occurred at or after the time of the termination peak. The pores themselves grew in size and joined together as hydration progressed and sometimes appeared to be aligned. In addition, high magnification images suggest that in some cases the pores appeared to undercut the surface of grain, preferentially growing in the bulk material (Figure 8). While the results shown here are similar in nature to those of Henderson and Bailey[30], the additional information on the surface behaviour and pore development leads to different conclusions about the cause of the end of the induction period. The different physical models for the induction period have been considered to fall into four types[14]:

- Models where the product of the initial reaction forms a protective layer on the C_3S, with the induction period ending when this layer is destroyed or rendered more permeable by aging or phase transformation[2-4];
- Models where the product of the initial reaction forms a semi-permeable membrane which encloses an inner solution and is destroyed by osmotic bursting[5,6];
- Models where the induction period does not exist as such, but rather the observed behaviour is due to the rate of nucleation and growth of the C-S-H initially being very slow and eventually reaching a critical point where acceleration occurs and the main reaction begins[7-10]; and
- Models where the induction period occurs due to calcium hydroxide nuclei being poisoned by the presence of SiO_2 and can not grow, with induction ending when the level of supersaturation of the solution is sufficient to overcome this effect[11, 12].

The second model has frequently been used in recent work[25,30,31,34].

None of the above generalized models appears to fit the data presented here precisely, although the first hypothesis is closest to what was observed. Hexagonal crystals that appear to be calcium hydroxide were identified in all of the materials examined even where hydration had been stopped well before the end of the induction period (Figure 7). In addition, differential scanning calorimetry has shown that calcium hydroxide forms in the hydration of C_3S as much as 60 minutes or more before the end of the induction period[15]. There would therefore not appear to be a connection between the end of the induction period and the initial formation of calcium hydroxide.

Models which assume that there is a continuous process of growth and nucleation that gradually accelerates over time do not explain the presence of either the termination peak in the

hydration curves (Figure 1b) or the corresponding rapid increase in observed porosity and hydration products (Figure 6). The presence of these effects indicate that cement hydration is not a monotonic process, but that there is an actual event that ends the induction period.

The physical appearance of the cement surface in Figures 6 and 8 does not support models that are based on osmotic pressure rupturing the surface of the protective layer. The pores in the surface of the grains have the appearance of being produced by dissolving the surface, not that of cracks or holes that have formed from interior pressure. Samples with longer periods of hydration also show larger pores, again suggesting a dissolution process. Further, hydration products on the surface of the grains are not directly associated with the pores observed in the surface. As an example, more of the white, rod like structures in Figure 6d were located in regions of the sample without pores than were located in porous regions, while many surfaces show pores without hydration products. With the exception of a single instance, a careful examination of samples at high magnifications did not show exact co-location of the pores and the hydration products. These results suggest that at a 0.5 w/c ratio the C-S-H is forming by nucleation on the surface of the grain, rather than around an osmotically produced pore. Examples have also been seen where C-S-H formation has initiated on the prismatic hydration products, again suggesting a nucleation formation process.

The final type of model, where a protective layer loses its protective capacity and becomes more permeable due to aging or phase transformation can not be confirmed or denied by the results of this study. There was insufficient resolution in the scanning electron microscopy images to show whether such a surface layer exists. If it does exist, the formation of the pores at the end of the induction period would suggest that the protective layer itself underwent localized

chemical attack, rather than experiencing a phase transformation or other event that causes a general increase in permeability.

Conclusion

High resolution isothermal conduction calorimetry has shown the presence of a peak in the hydration reactions at the end of the induction period in both C_3S[15] and Type I and Type I/II OPC. CFE-SEM imaging showed that during this time period, a rapid formation of pores occurred in the surface of the cement grains, as well as a rapid formation of C-S-H. The pores were initially 4 nm or smaller in diameter, but grew in size in the hours after the end of the induction period. Similar results were observed in all examined samples, including those where the heat flow generated by C_3A hydration masked the termination peak in the isothermal conduction calorimetry measurements. While the size of the termination peak in C_3S was controlled by the surface area of the anhydrous material, in Portland cements the hydration products of C_3A and C_4AF play a significant role in the peak's development by preventing the formation of C-S-H on the surface of the cement grains.

Existing models for the induction period do not fit well with the observed OPC hydration behaviour. Calcium hydroxide was observed to form on the cement grains well before the end of the induction period. The pores that form in surface of the grain had the appearance of being produced by chemical attack and dissolution, rather than that of damage produced by osmotic pressure. As a result, a comparison with the existing models for the causes of the induction period and its end showed that the experimental results do not support models based on formation of calcium hydroxide, osmotic bursting or slow nucleation and growth of C-S-H. Although the observed behaviour fits to some extent with those models where the induction period ends when a protective layer on the surface of the cement breaks down, no direct observation of such a layer

was obtained and the observed process of pore formation does not support the concept of a general increase in permeability of such a protective layer. The differences between the existing models of the induction period and the results of this study suggest that further work is needed towards understanding the mechanisms associated with this period in the OPC hydration process.

Acknowledgements

The Rietveld analysis of cement chemical composition was provided by L.D. Mitchell. K. Esseghaier and J. Margeson prepared the freeze-dried samples. Ken Trischuk performed the BET surface measurements.

References

1. A.M. Neville, p. 13 in *Properties of Concrete*, 4th Edition, Pearson Education Limited, Harlow, Essex, UK (1995).
2. P.W. Brown, K. Galuck and G. Fronsdorff, "A kinetic model for the hydration of tricalcium silicate", *Cem. Concr. Res*., 15 35-41 (1985).
3. H.M. Jennings, "Aqueous solubility relationships for two types of calcium silicate hydrate", *J. Am. Ceram. Soc.*, 69 [8] 614-618 (1986).
4. H.N. Stein and J.M. Stevels, "The influence of silica on the hydration of $3CaO,SiO_2$", *J. Appl. Chem.*, 14, 338-346, (1964).
5. D.D. Double, "New developments in understanding the chemistry of cement hydration", *Phil. Trans. R. Soc. Lond.* A310 53-66 (1983).
6. J.D. Birchall, A.J. Howard and J.E. Bailey, "On the hydration of Portland cement", *Proc. R. Soc. Lond.* A360, 445-453, (1978).
7. P. Barret, D. Bertrandie and D. Ménétrier, "Etude comparée de la formation de C-S-H à partir de solutions sursaturees et de mélanges C_3S solution, pp 261-272 in *Proceedings of the 7th International Congress on Chemistry of Cement*, Vol. 2, Part 2, Editions Septima, Paris (1980).
8. P. Fierens and J.P. Verhagen, "Hydration of tricalcium silicate in paste — Kinetics of calcium ions dissolution in the aqueous phase", *Cem. Concr. Res*., 6 337-342 (1976).
9. I. Odler and H. Dörr, "Early hydration of tricalcium silicate II. The induction period", *Cem. Concr. Res.*, 9 277-284 (1979).

10. R. Sierra, "Contribution to the kinetic study of hydration of tricalcium silicate", in *Proceedings of the 6th International Congress on the Chemistry of Cement*, Supplementary Papers, Part II, Section 2, Stroyizdat, Moscow (1976).
11. M.E. Tadros, J. Skalny and R.S. Kalyoncu, "Early Hydration of Tricalcium Silicate", *J. Am. Ceram. Soc.*, 59 [7-8] 344-347 (1976).
12. Z.-Q. Wu, and J.F. Young, "Formation of Calcium Hydroxide from Aqueous Suspensions of Tricalcium Silicate", *J. Am. Ceram. Soc.*, 67 [1] 48-52 (1984).
13. H.F.W Taylor et al., "The hydration of tricalcium silicate", *Materiaux et Constructions*, 17 457-468 (1984).
14. H.F.W Taylor, p. 153 in *Cement Chemistry* 2nd Ed., Thomas Telford, London (1997)
15. J.M. Makar, G.W. Chan, and K.Y. Esseghaier, "An Additional Hydration Reaction at the End of the Cement Induction Period", *J. Mater. Sci.,* 42 1388-1392 2007.
16. P. Longuet, Proceedings of the Fifth International Symposium on the Chemistry of Cement (Tokyo, Oct 7-11, 1968), Part II, vol. II 30 1969.
17. I.G. Richardson and G.W. Groves, "Microstructure and microanalysis of hardened ordinary Portland cement pastes", *J. Mater. Sci.*, vol. 28 265-277 (1993).
18. C. Gallé, "Effect of drying on cement-based materials pore structure as identified by mercury intrusion porosimetry: A comparative study between oven-, vacuum-, and freeze drying", *Cem. Concr. Res.*, 31 1467-1477 (2001).
19. A. Korpa and R. Trettin, "The influence of different drying methods on cement paste microstructures as reflected by gas adsorption: Comparison between freeze-drying (F-drying), D-Drying , P-drying and oven drying methods", *Cem. Concr. Res.*, 36 634-649 (2006).

20. S. Diamond, "Cement paste microstructure – An overview at several levels", pp 3-23 in *Hydraulic Cement Pastes: Their Structure and Properties*, Cement and Concrete Association, Wexham Springs, Slough, UK (1976).

21. B.J. Dalgliesh, P.L. Pratt and E.J. Toulson, "Fractographic Studies in Microstructure Development of Hydrated Portland Cement", *J. Mater. Sci.*, 17 [8] 2199-2207 (1982).

22. H.M. Jennings, B.J. Dalgliesh and P.L. Pratt, "Morphological Development of Hydrating Tricalcium Silicate as Examined by Electron Microscopy Techniques", *J. Am. Ceram. Soc.*, 64 [10] 567-572 (1981).

23. D. Ménétrier, I. Jawed, T.S. Sun and J. Skalny, "ESCA and SEM studies on early C_3S hydration", *Cem. Concr. Res*., 9 473-482 (1979).

24. P.L. Pratt and A. Ghose, "Electron microscopy studies of Portland cement microstructures during setting and hardening", *Phil. Trans. R. Soc. Lond.*, A310, 93-103 (1983).

25. P. Meredith, A.M. Donald and K. Luke, "Pre-induction and induction hydration of tricalcium silicate: an environmental scanning electron microscopy study", *J. Mater. Sci.*, 30 1921-1930 (1995).

26. J. Stark, B. Möser, and A. Eckart, "New approaches to cement hydration, part 1", *ZKG Inter.*, 54 [1] 52-60 (2001).

27. J. Stark, B. Möser, and A. Eckart, "New approaches to cement hydration, part 2", *ZKG Inter.*, 54 [2] 114-119 (2001).

28. F. Goetz-Neunhoeffer, J. Neubauer and P. Schwesig, "Mineralogical characteristics of Ettringites synthesized from solutions and suspensions", *Cem. Concr. Res*., 36 65-70 (2006).

29. H.F.W Taylor, p. 168 in *Cement Chemistry* 2nd Ed., Thomas Telford, London (1997)

30. E. Henderson and J.E. Bailey, “The compositional and molecular character of the calcium silicate hydrates formed in the paste hydration of $3CaO{\cdot}SiO_2$”, *J. Mater. Sci.* 28 3681-3691 (1993).

31. S.M. Clark, G.R. Morrison and W.D. Shi, “The use of scanning transmission X-ray microscopy for the real time study of cement hydration”, *Cem. Concr. Res.*, 29 1099-1102 (1999).

32. M.C.G. Juenger, V.H.R. Lamour, P.J.M. Monterio, E.M. Gartner, and G.P. Denbeaux, “Direct observation of cement hydration by soft X-ray transmission microscopy”, *J. Mater. Sci. Let.*, 22 1335-1337 (2003).

33. M.C.G. Juenger, P.J.M. Monterio, E.M. Gartner, and G.P. Denbeaux, “A soft X-ray microscope investigation into the effects of calcium chloride on tricalcium silicate hydration”, *Cem. Concr. Res*., 35, 19-25 (2005).

34. L.D. Mitchell, M. Prica and J.D. Birchall, “Aspects of Portland cement hydration studied using atomic force microscopy”, *J. Mater. Sci*., 31 4207-4212 (1996).

Tables

Component	Lafarge 2004 OPC		St. Lawrence 2005 OPC		Maritime 1974 NPC	
	Weight %	uncertainty	Weight %	uncertainty	Weight %	uncertainty
$3CaO{\cdot}SiO_2$	67.5	0.94	66.68	0.81	76.56	0.84
$2CaO{\cdot}SiO_2$	9.06	0.72	12	0.65	10.16	0.66
$4CaO{\cdot}Al_2O_3{\cdot}Fe_2O_3$	9.04	0.51	7.07	0.48	3.68	0.29
$3CaO{\cdot}Al_2O_3$	2.98	0.16	3.66	0.13	5.5	0.16
$CaCO_3$	3.48	0.39	4.28	0.3	1.36	0.26
MgO	1.11	0.17	1.02	0.15	0.29	0.1
SiO_2	0.096	0.084	0.674	0.08	0.322	0.096
Free CaO	0.58	0.73	0.429	0.093	0.373	0.055
$CaSO_4{\cdot}2H_2O$	2.69	0.34	2.46	0.15	0.93	0.21
$CaSO_4{\cdot}½H_2O$	2.74	0.29	1.56	0.24	0.82	0.17
Anhydrous $CaSO_4$	0.73	0.23	0.16	0.15	0	
Total	100.006		99.993		99.995	

Table 1: Constituents by Rietveld analysis of OPC and NPC used in the experiment. Totals do not precisely equal to 100% due to rounding errors.

Portland Cement	Covered area of grain
Lafarge 2004 (1.22 m^2/g)	20%
St. Lawrence 2005	48%
Maritime 1974	24%
Lafarge 2004 (3.29 m^2/g)	31%
80% Lafarge 2004, 20% C_4AF	34%

Table 2: Average surface area covered by pre-induction hydration products

Figure Captions

Figure 1: Isothermal conduction calorimetry results for OPC and NPC: a) full data set; b) initial hydration period. The small dots in b) represent individual data points, while the large symbols indicate points where the hydration of the cement was stopped for imaging.

Figure 2: Effect on heat of hydration during the induction period of additions of a) C_3A and b) C_4AF to Lafarge 2004 OPC during the induction period

Figure 3: Effect on heat of hydration during the induction period of increasing OPC fineness (Lafarge 2004 OPC)

Figure 4: Comparison between a) 20kV and b) 2.0 kV images, St. Lawrence OPC, 180 minutes hydration [4.9 mm working distance]

Figure 5: Examples of unhydrated St. Lawrence 2005 OPC at 2.0 kV with: a) generally smooth surfaces with adhered particles [2.9 mm working distance]; b) damaged surfaces [2.8 mm working distance]

Figure 6: Morphology of St. Lawrence 2005 OPC at different times of hydration [3.0 mm working distance, 1.5 keV]: a) 90 minutes; b) 105 minutes, immediately before termination peak; c) 120 minutes, at termination peak (pore formation - arrow); d) 120 minutes at termination peak (C-S-H clusters); e) 180 minutes (example of increased porosity); f and g) 180 minutes (typical C-S-H forms); h & i) 240 minutes.

Figure 7: Calcium hydroxide formation, Lafarge 2004 OPC, 30 minutes hydration (induction period) [3.0 mm working distance, 1.5 kV, arrows indicate hydration products]

Figure 8: Pore structure at 360 minutes hydration (Lafarge 2004 OPC) showing growth of pores and possible below surface pore connections [3.0 mm working distance, 1.5 kV].

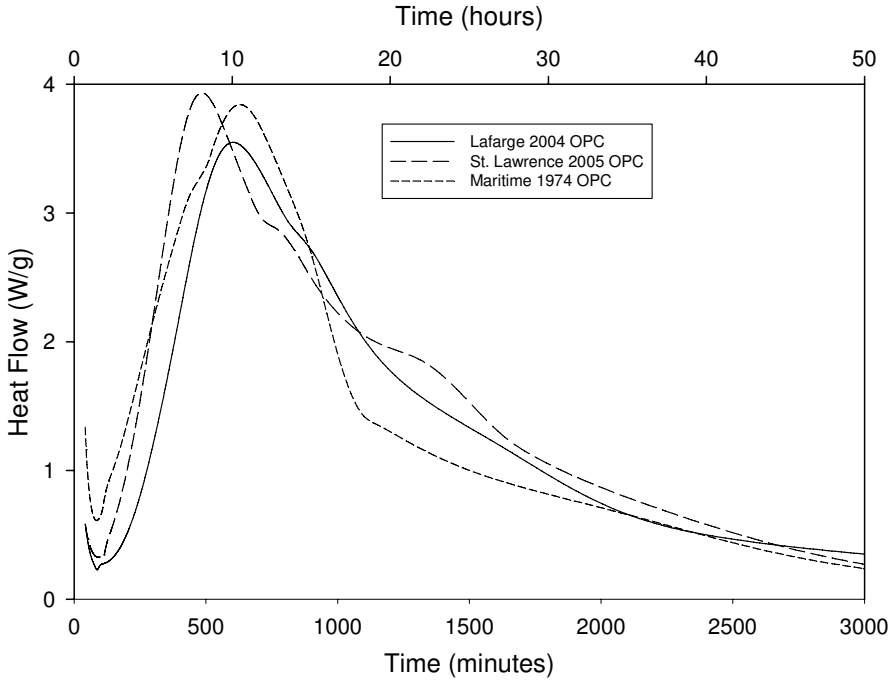

1a)

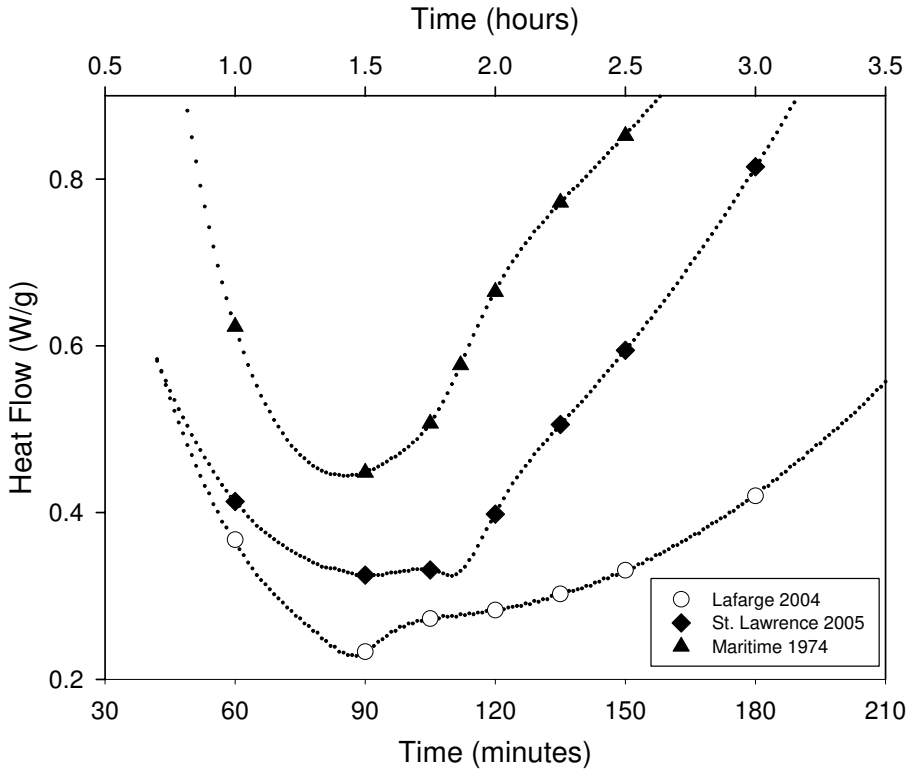

1b)

Figure 1: Isothermal conduction calorimetry results for OPC and NPC: a) full data set; b) initial hydration period. The small dots in b) represent individual data points, while the large symbols indicate points where the hydration of the cement was stopped for imaging.

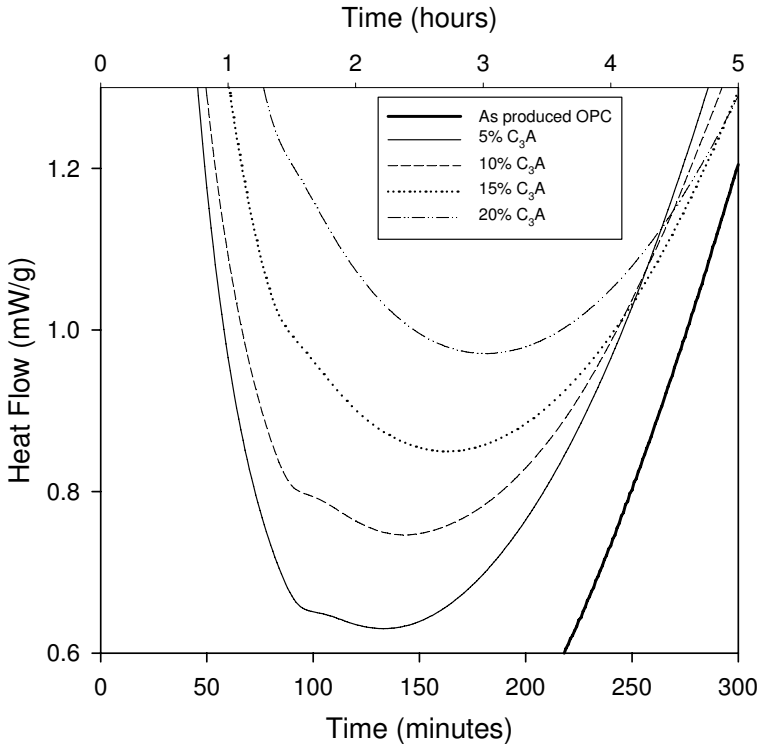

2a)

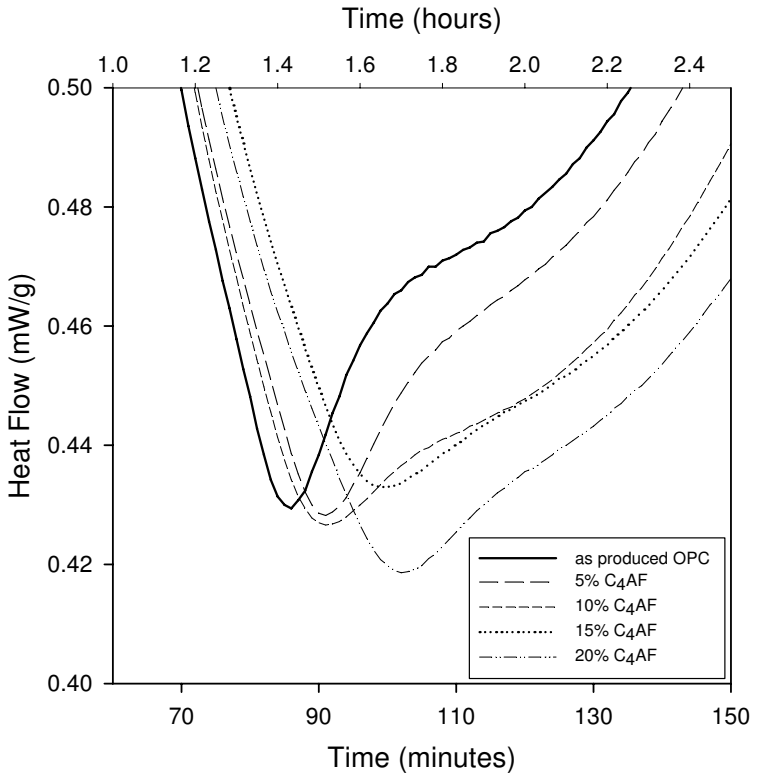

2b)

Figure 2: Effect on heat of hydration during the induction period of additions of a) C_3A and b) C_4AF to Lafarge 2004 OPC during the induction period

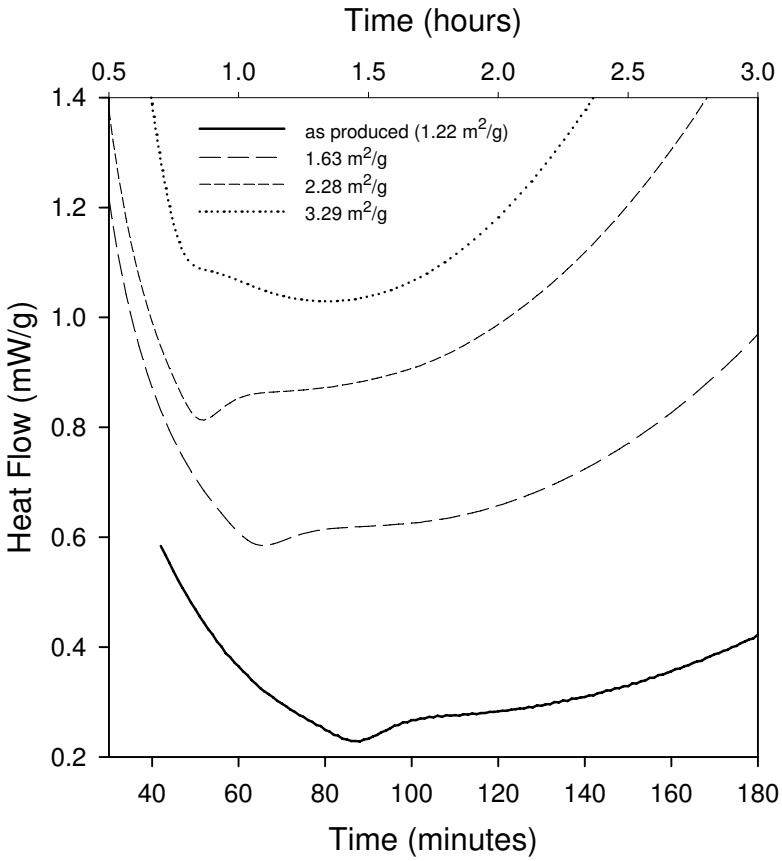

Figure 3: Effect on heat of hydration during the induction period of increasing OPC fineness (Lafarge 2004 OPC)

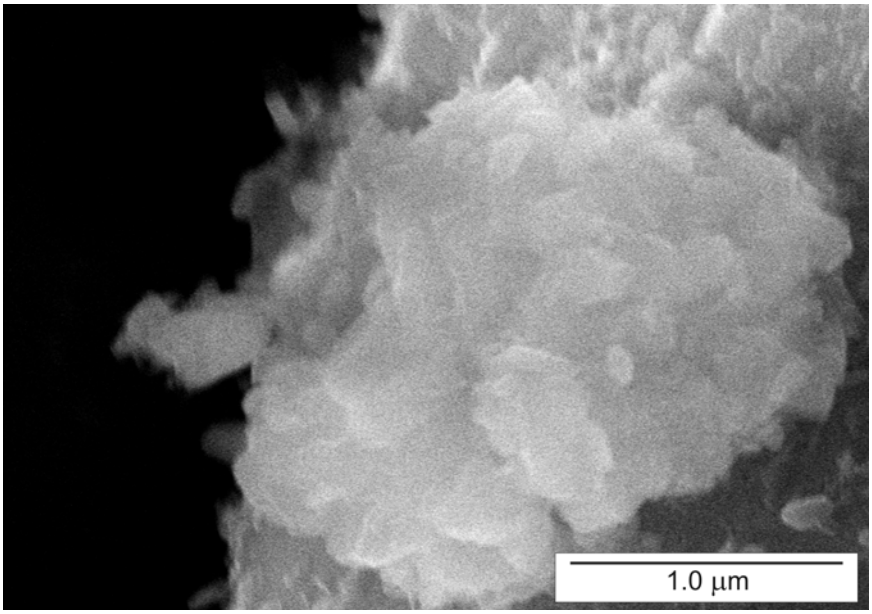

4a)

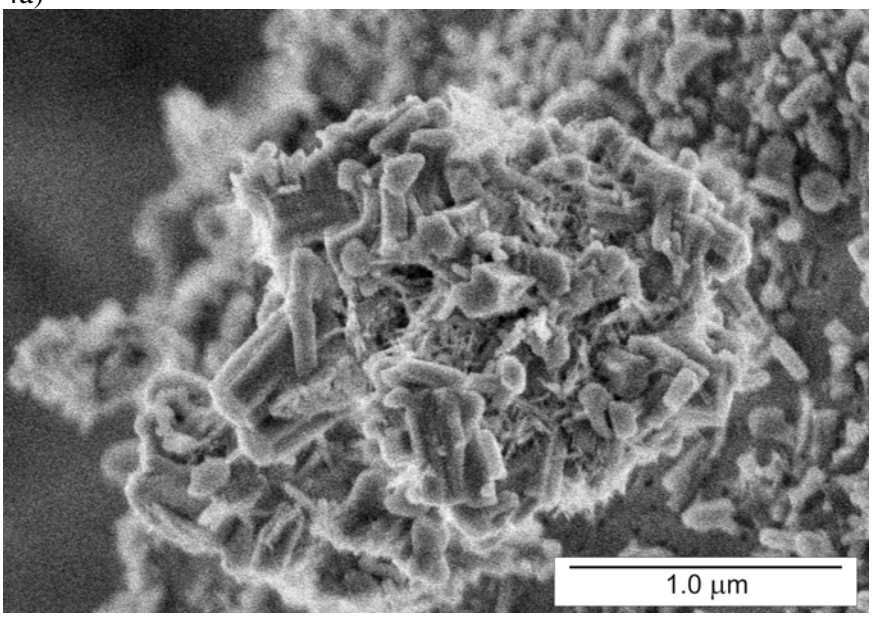

4b)

Figure 4: Comparison between a) 20kV and b) 2.0 kV images, St. Lawrence OPC, 180 minutes hydration [4.9 mm working distance]

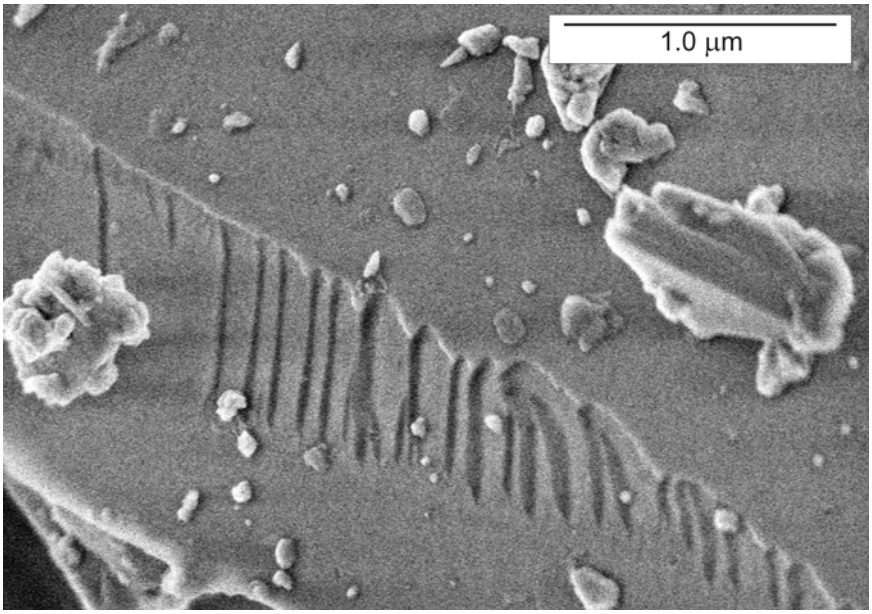

5a)

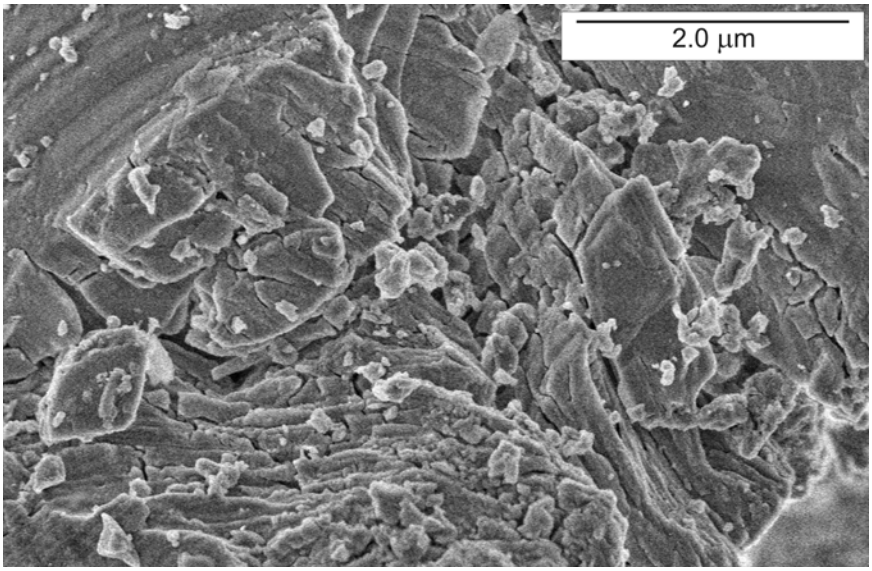

5b)

Figure 5: Examples of unhydrated St. Lawrence 2005 OPC at 2.0 kV with: a) generally smooth surfaces with adhered particles [2.9 mm working distance]; b) damaged surfaces [2.8 mm working distance]

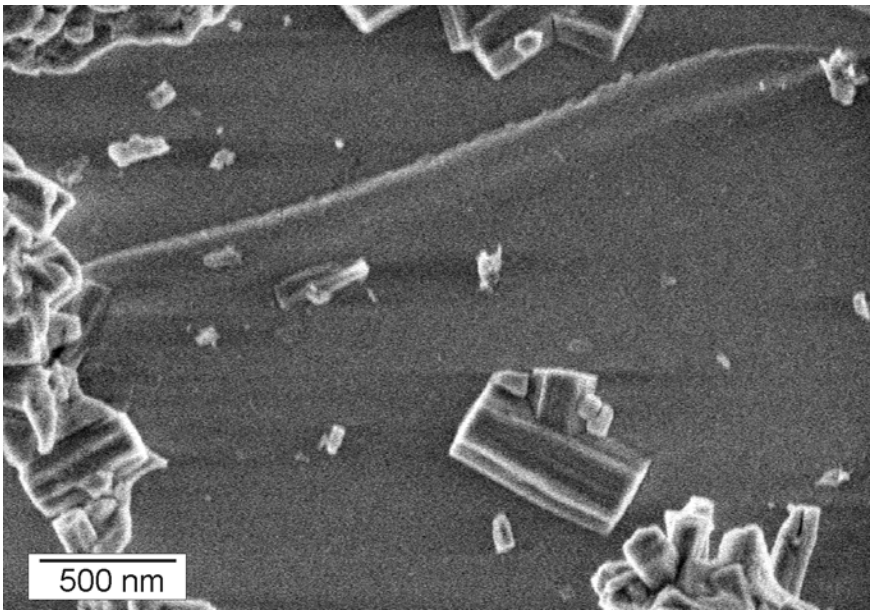

6a)

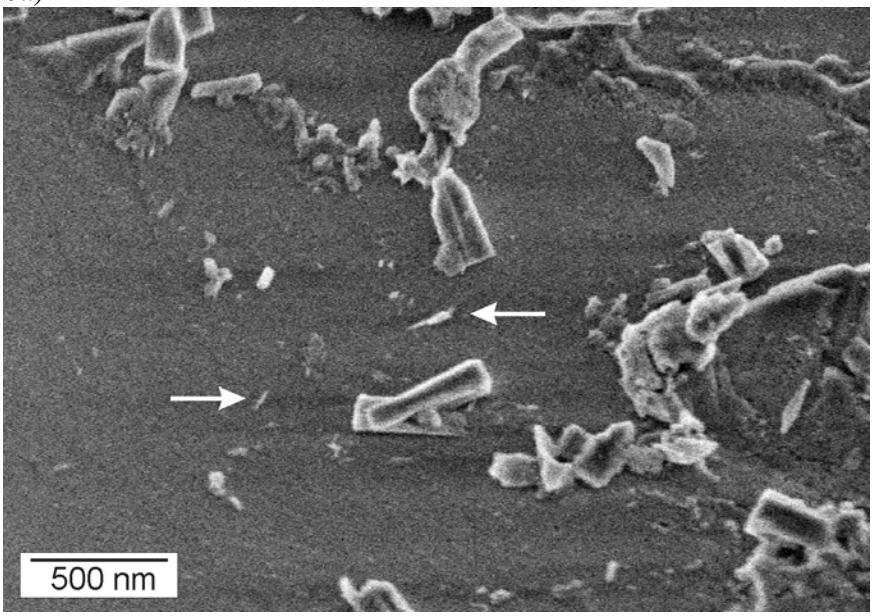

6b)

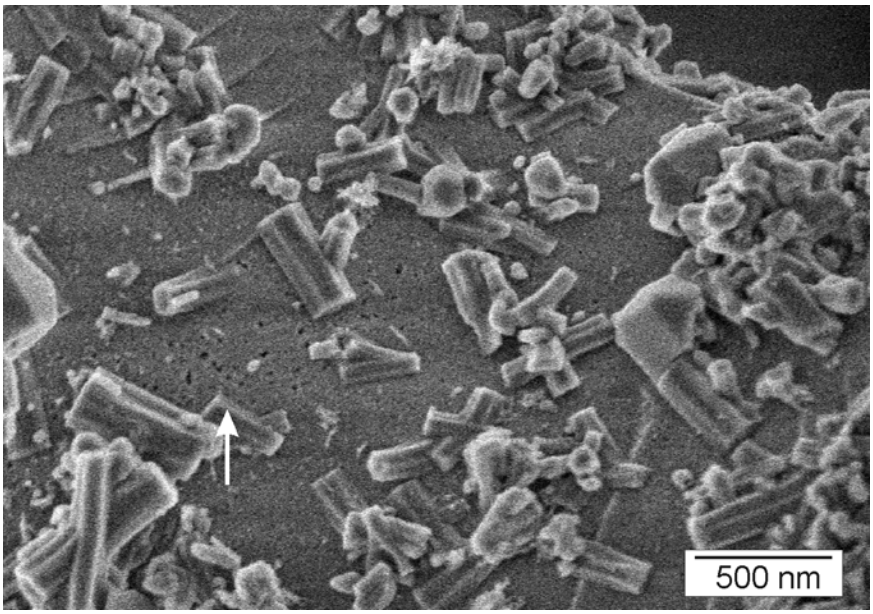

6c)

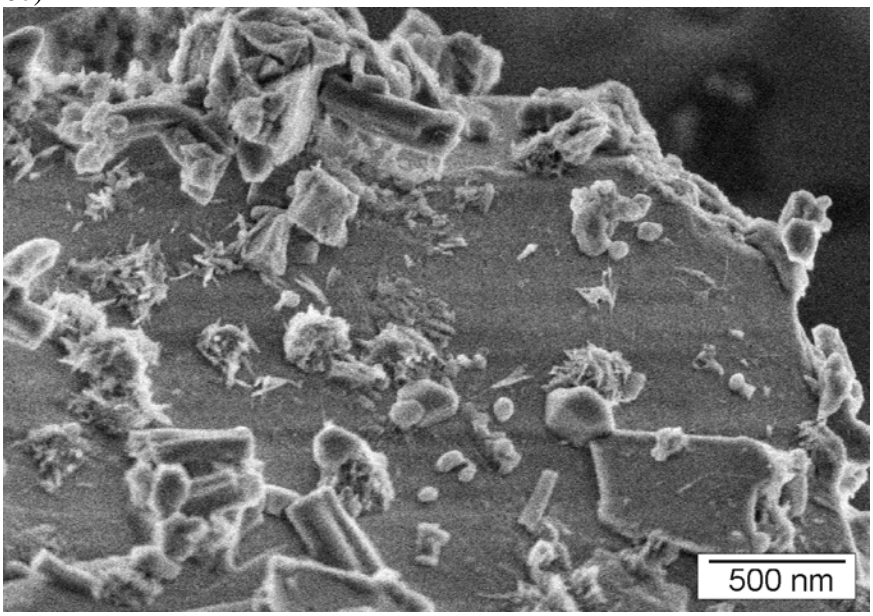

6d)

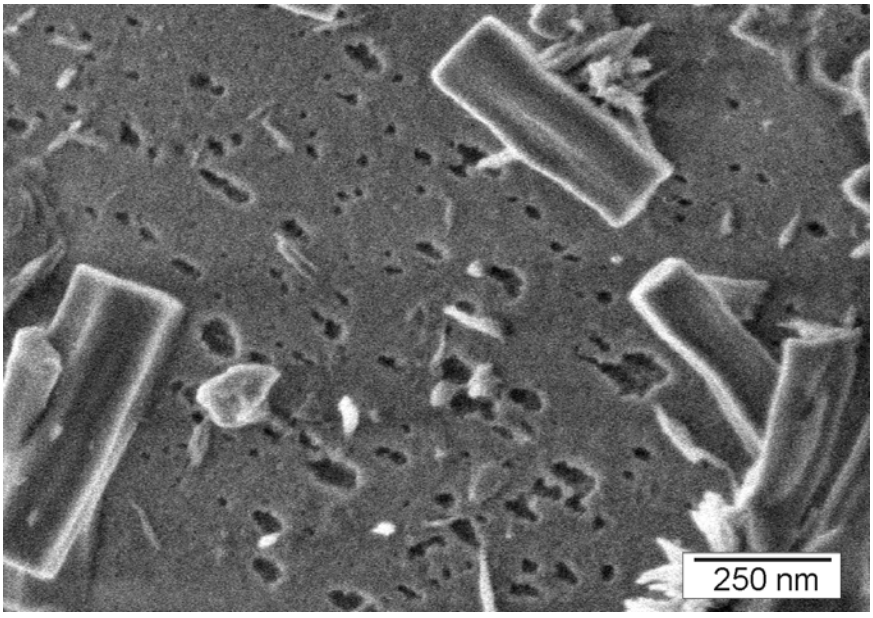

6e)

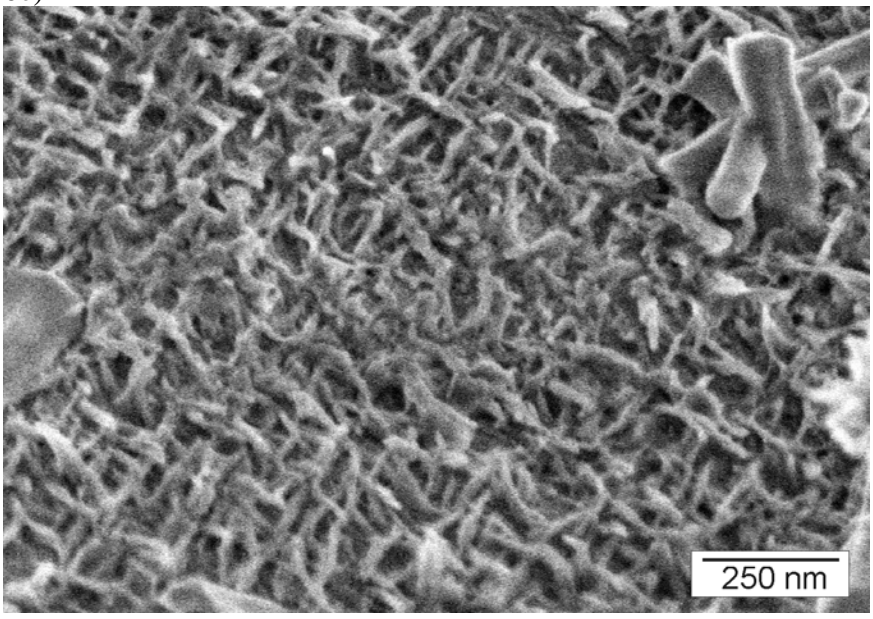

6f)

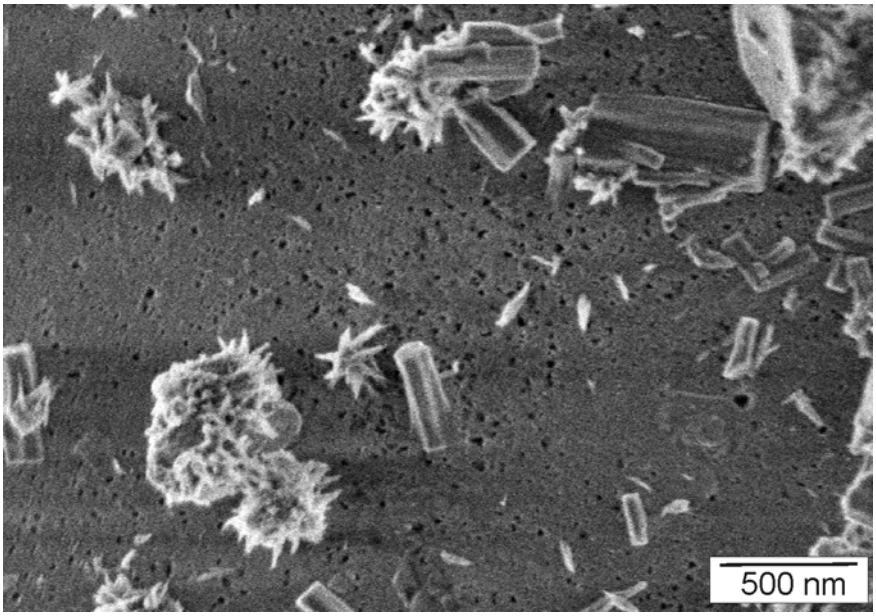

6g)

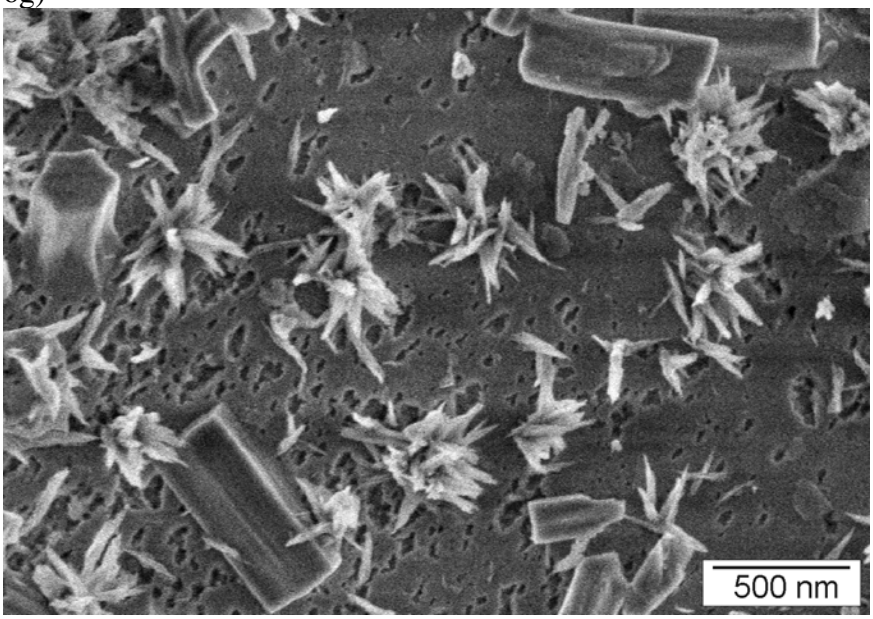

6h)

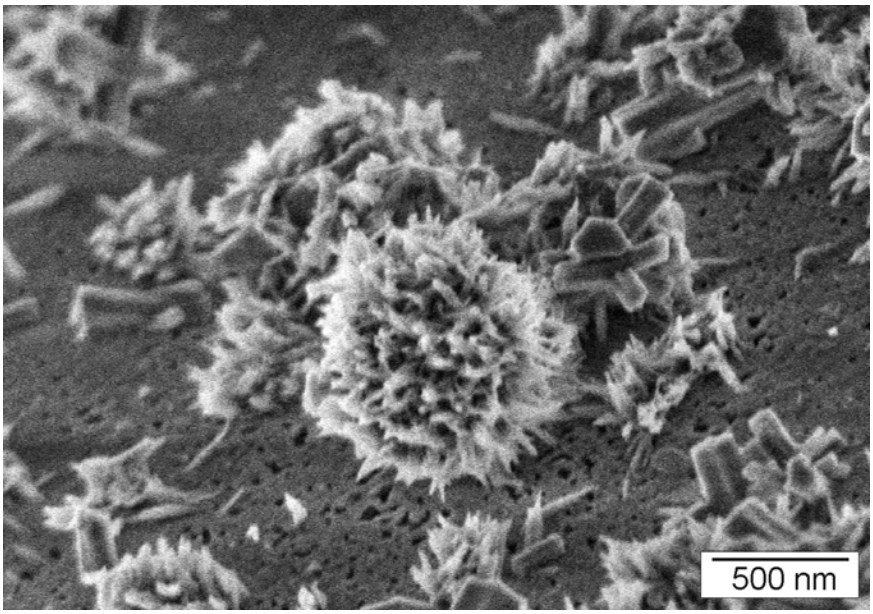

6i)

Figure 6: Morphology of St. Lawrence 2005 OPC at different times of hydration [3.0 mm working distance, 1.5 keV]: a) 90 minutes; b) 105 minutes, immediately before termination peak; c) 120 minutes, at termination peak (pore formation - arrow); d) 120 minutes at termination peak (C-S-H clusters); e) 180 minutes (example of increased porosity); f and g) 180 minutes (typical C-S-H forms); h &i) 240 minutes.

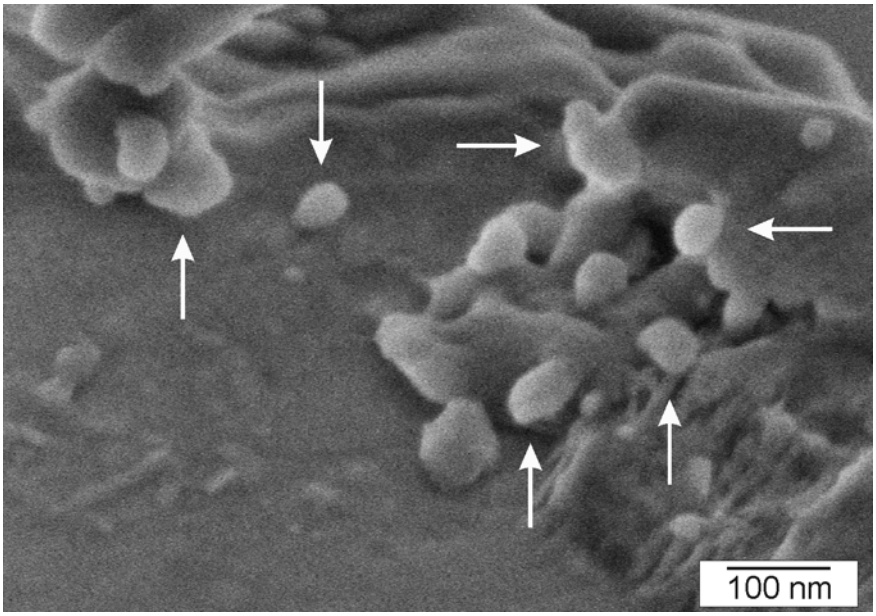

Figure 7: Calcium hydroxide formation, Lafarge 2004 OPC, 30 minutes hydration (induction period) [3.0 mm working distance, 1.5 kV]

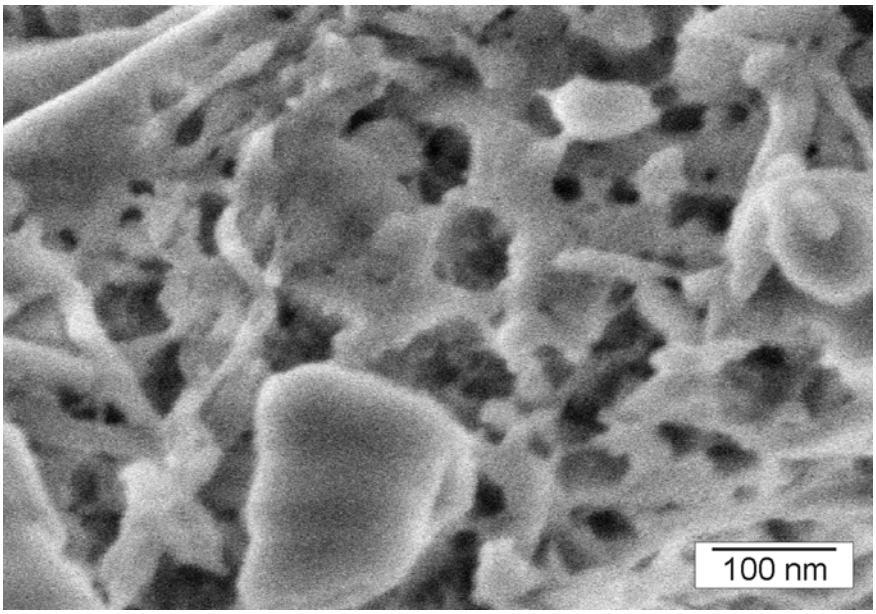

Figure 8: Pore structure at 360 minutes hydration (Lafarge 2004 OPC) showing growth of pores and possible below surface pore connections [3.0 mm working distance, 1.5 kV].